 doi:10.20944/preprints202104.0246.v1

Article

Study of dependence of kinetic freezeout temperature on production cross-section of the particles in various centrality intervals in Au-Au and Pb-Pb collisions at high energies

Muhammad Waqas [1], Guang Xiong Peng [2]

[1] School of Nuclear Science and Technology, University of Chinese Academy of Sciences, Beijing 100049, China; waqas_phy313@yahoo.com or waqas_phy313@ucas.ac.cn
[2] Theoretical Physics Center for Science Facilities, Institute of High Energy Physics, Beijing 100049, China; gxpeng@ucas.ac.cn

Abstract: Transverse momentum spectra of π^+, p, Λ, Ξ or $\bar{\Xi}^+$, Ω or $\bar{\Omega}^+$ and deuteron (d) in different centrality intervals in Gold-Gold (Au-Au) and Lead-Lead (Pb-Pb) collisions at 62.4 GeV and 2.76 TeV respectively, are analyzed by the blast wave model with Boltzmann Gibbs statistics. We extracted Kinetic freeze out temperature, transverse flow velocity and kinetic freezeout volume from the transverse momentum spectra of the particles. It is observed that the non-strange and strange (multi-strange) particles freezeout separately due to different reaction cross-sections. While the freezeout volume and transverse flow velocity are mass dependent which decrease with the rest mass of the particles. The present work reveals the scenario of double kinetic freezeout in collisions at STAR and ALICE Collaborations. Furthermore, the kinetic freezeout temperature and freezeout volume are larger in central collisions than the peripheral collisions and they decrease from central to periphery. However the transverse flow velocity remains almost unchanged from central to peripheral collisions.

Keywords: non-strange; strange; multi-strange; kinetic freeze-out temperature; transverse flow velocity; freezeout volume; cross-section; centrality bins; transverse momentum spectra

PACS: 12.40.Ee, 13.85.Hd, 25.75.Ag, 25.75.Dw, 24.10.Pa

1. Introduction

Freezeout stages are very important because they provide essential information about the emission of the particles at those stages. Generally, there are two freeze-out stages found in literature namely chemical freezeout and kinetic freezeout stage. Both these freezeout stages correspond to their respective temperatures. The chemical freezeout is the intermediate stage in high energy collisions where the intra-nuclear collisions among the particles are inelastic and the ratios of various types of particles remain unchanged and the temperature of the particles at this stage is chemical freezeout temperature that describes the excitation degree of the system at the chemical freezeout stage. Correspondingly, the thermal/kinetic frrzeout is the last but not the least stage in high energy collisions. At this stage, the intra- nuclear collisions among the particles are elastic and the transverse momentum distributions of various kinds of particles are no longer changed and the temperature at this stage is called kinetic freezeout temperature.

According to thermal and statistical model [1–4], the chemical freezeout temperature (T_{ch}) in central nucleus- nucleus collisions increases with increase of the collisions energy from a few GeV to above 10 GeV and then saturates in an energy range from more than a dozen of GeV. At top Relativistic Heavy Ion Collider (RHIC) and Large Hadron Collider (LHC), the maximum T_{ch} is 160 MeV, although there is a slight increase from RHIC to LHC energy, but the situation of kinetic freezeout temperature (T_0) is complex. At first, T_0 in central collisions increases with increasing the collision energy from a few GeV to

Preprints (www.preprints.org) | NOT PEER-REVIEWED | Posted: 8 April 2021 doi:10.20944/preprints202104.0246.v1

above 10 GeV, but this tendency can either be saturated, decrescent or increscent. On the other hand, T_{ch} central nucleus-nucleus collisions is abit larger than in peripheral nucleus-nucleus collisions, however, there are three possible trends of T_0 from central to peripheral collisions which are (1) T_0 increase from central to peripheral collisions (2)T_0 decrease from central to peripheral collisions and (3) T_0 remains constant from central to peripheral collisions. It is very important to search for the correct trend of T_0 with energy and centrality. Furthermore, there are different kinetic freezeout scenarios found in literature which include single, double, triple and multiple kinetic freezeout scenarios [5–10]. In single kinetic freezeout scenario one set of parameters is used for the strange, multi-strange and non-strange particles, in double kinetic freezeout scenario one set of parameters is used for strange (multi-strange) and other for non-strange particles, separate sets of parameters are used for strange, multi-strange and non-strange particles in triple kinetic freezeout scenario, while separate sets of parameters for each particle are used in multiple kinetic freezeout scenario. The trend of transverse flow velocity (β_T) and freezeout volume (V) with energy is an increasing trend in most of the literatures [6, 11-16]. Most of the literature claims the decreasing (or invariant) trend of β_T and V from central to peripheral collisions [10, 15, 16–18].

The transverse momentum spectra (p_T) of the particles are very important observables due to the reasons that they provide very essential information about the equilibrium dynamics and isotropy of the system in high energy collisions [9]. In present work, we will analyze the p_T spectra of π^+, p, Λ, Ξ ($\bar{\Xi}^+$), Ω ($\bar{\Omega}^+$) and deuteron (d) in Au-Au and Pb-Pb collisions at 62.4 GeV and 2.76 TeV respectively.

The remainder of the paper consists of method and formalism, and results and discussion in section 2 and 3 respective;y and the summary our main observations and conclusions are presented in section 4.

2. The method and formalism

There are various models suggested for the extraction of T_0, V and β_T, e:g blast wave model with Boltzmann Gibbs statistics (BGBW) [19–21], blast wave model with Tsallis statistics [TBW] [22–24], an alternative method by using Tsallis statistics [25–31] and an alternative method by using blast wave model boltzmann Gibbs statistics [32–37]. In this work, we choose the blast wave model with boltzmann Gibbs statistics which is phenomenological model and is used for the spectra of hadrons based on the flow of local thermal sources with global variables of temperature, volume and transverse flow velocity.

According to reference [38–40], the p_T distribution of the BGBW can be written as

$$f(p_T) = \frac{1}{N}\frac{dN}{dp_T} = C\frac{gV}{(2\pi)^2} p_T m_T \int_0^R r dr \times I_0\left[\frac{p_T \sinh(\rho_1)}{T_0}\right] K_1\left[\frac{m_T \cosh(\rho_1)}{T_0}\right], \quad (1)$$

where C stands for the normalization constant, g represents the degeneracy factor of the particles, V is the freezeout volume, $m_T = \sqrt{p_T^2 + m_0^2}$ is the transverse mass, m_0 is the rest mass of the particle, r is the radial coordinate, R is the maximum r, $\rho = \tanh^{-1}[\beta(r)]$ is the boost angle, $\beta(r) = \beta_S(r/R)^{n_0}$ is a self-similar flow profile, β_S is the flow velocity on the surface, as mean of $\beta(r)$, $\beta_T = (2/R^2)\int_0^R r\beta(r)dr = 2\beta_S/(n_0+2)$, and n_0 is regarded as free parameter [41] that fluctuates largely by several times increases 1 in the number of free parameters. I_0 and K_1 are the bessel modified functions of the first and second kind respectively.

Eqn. (1) is not enough for the description of the whole p_T spectra, particularly, when the maximum p_T reaches to 100 GeV/c at LHC collisions [42], where several p_T regions [43] has been observed by the model analysis. These regions include the first p_T region with p_T <4.5 GeV/c, the second region and third region with 4-6 GeV/c < p_T <

Preprints (www.preprints.org) | NOT PEER-REVIEWED | Posted: 8 April 2021 doi:10.20944/preprints202104.0246.v1

17-20 GeV/c and $p_T >$ 17-20 GeV/c respectively. Different p_T regions are expectedly in correspondence to different interacting mechanisms, such as the effects and changes by medium, nuclear transparency and the effect of number of strings etc, which are discussed in detail in [17]. Therefore, for the complete description of the whole p_T, we can use the functions such as Tsallis Levy [44, 45], the Hagedorn function [42, 46, 47] to the spectra in high and very high p_T regions and it corresponds to an the inverse power law. In this work, we used the inverse power law to describe the p_T spectra in high p_T regions, that is

$$f_H(p_T) = \frac{1}{N}\frac{\mathrm{d}N}{\mathrm{d}p_\mathrm{T}} = Ap_T\left(1+\frac{p_T}{p_0}\right)^{-n}, \tag{2}$$

where N and A represents the number of particles and normalization constant respectively, and p_0 and n are the free parameters. There are several modified versions of Hagedorn function found in literature [48–54].

Generally, the two main process responsible for the contribution of p_T spectra are soft excitation (contributes soft component in low p_T region) and hard scattering process (contributes in whole p_T region). Eqn. (1) is taken into account for the soft excitation process and eqn.(2) for the hard scattering process. Eqn. (1) and (2) can be superposed by (1)super position principle where the contribution regions of components overlap each other and (2) by hagedorn model (usual step function), when there is no overlapping of different regions of different components. According to the first method

$$f_0(p_T) = kf_S(p_T) + (1-k)f_H(p_T), \tag{3}$$

where k represents the contribution fraction of the first component and (1-k) represents the contribution function of the second component.

The usual step function can be used to structure the superposition of the Eqn. (1) and (2). According to Hagedorn model [42, 46, 47], the usual step function can also be used for the superposition of the two functions, as

$$f_0(p_T) = A_1\theta(p_1-p_T)f_1(p_T) + A_2\theta(p_T-p_1)f_2(p_T), \tag{4}$$

where A_1 and A_2 are the fraction constants which give the two components to be equal to each other at p_T=p_1.

3. Results and discussion

Figure 1 demonstrates the transverse momentum (p_T) spectra, $[(1/2\pi p_T)\, d^2N/dydp_T]$ or $[1/N_{ev}(1/2\pi p_T)\, d^2N/dydp_T]$ of π^+, p, Λ, $\bar{\Xi}^+$, $\bar{\Omega}^+$ and deuteron (d) in various centrality classes in Au-Au collisions at 62.4 GeV. The spectra is distributed in different centrality classes, e:g for π^+ and p, 0–5%, 5–10%, 10–20%, 20–30%, 30–40%, 40–50%, 50–60%, 60–70% and 70–80%, for Λ, 0–5%, 5–10%, 10–20%, 20–30%, 30–40%, 40–60% and 60–80%, for $\bar{\Xi}^+$, 0–5%, 5–10%, 10–20%, 20–40%, 40–60% and 60–80%, for $\bar{\Omega}^+$, 0–20%, 20–40% and 40–60% at $|y| < 0.1$, and for deuteron (d), 0–10%, 10–20%, 20–40%, 40–60% and 60–80%, at $|y| < 0.3$. The symbols are cited from the experimental data measured by the STAR Collaboration at Relativistic Heavy Ion collisions (RHIC) [55-57]. In the figure, the curves are our fitted results with Eq. (1). The corresponding values of free parameters (T_0, V, β_T and n_0), normalization constant (N_0), χ^2 and number of degree of freedom (ndof) are listed in Table 1 in which the parameter trend will be analyzed and discussed later in this section. One can see that the p_T spectra of the particles are shown to obey approximately the blast wave model with boltzmann Gibbs statistics. Furthermore, the spectra of π^+ in 5–10%, 10–20%, 20–30%, 30–40%, 40–50%, 50–60%, 60–70% and 70–80% centrality intervals are scaled with 1/3, 1/7, 1/18, 1/40, 1/100, 1/250, 1/700 and 1/1500 respectively, while the centrality intervals of p 5–10%, 10–20%,

Preprints (www.preprints.org) | NOT PEER-REVIEWED | Posted: 8 April 2021 doi:10.20944/preprints202104.0246.v1

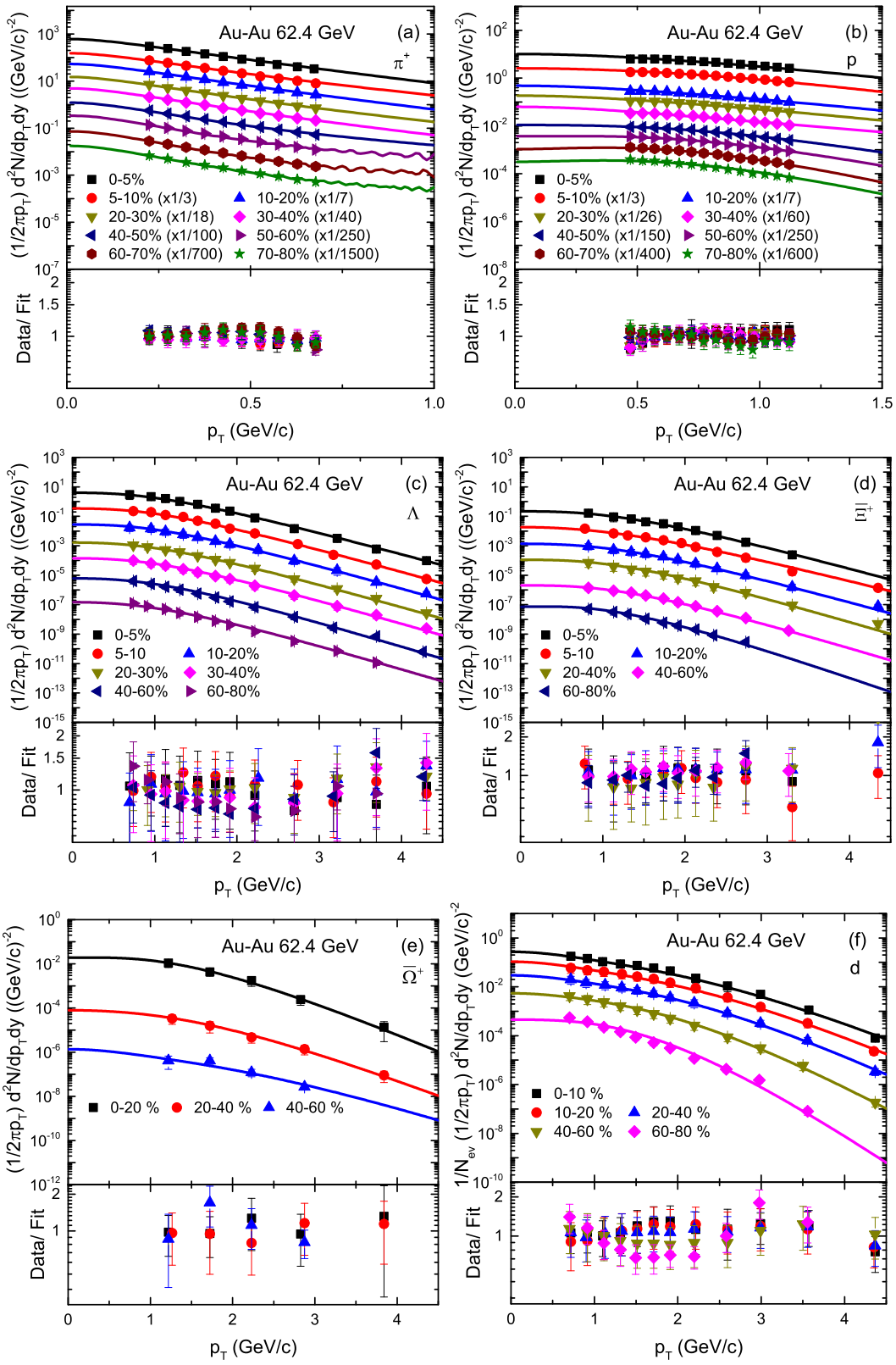

Fig. 1. Transverse momentum spectra of π^+, p, Λ, $\bar{\Xi}^+$ and $\bar{\Omega}^+$ rapidity $|y| < 0.1$, and deuteron (d) at rapidity $|y| < 0.3$, produced in different centrality intervals in Au-Au collisions at 62.4 GeV. Different symbols represent the p_T spectra of different particles measured by the STAR collaboration [55–57] and the curves are our fitted results with BGBW model. The corresponding results of data/fit is presented in each panel.

Preprints (www.preprints.org) | NOT PEER-REVIEWED | Posted: 8 April 2021 doi:10.20944/preprints202104.0246.v1

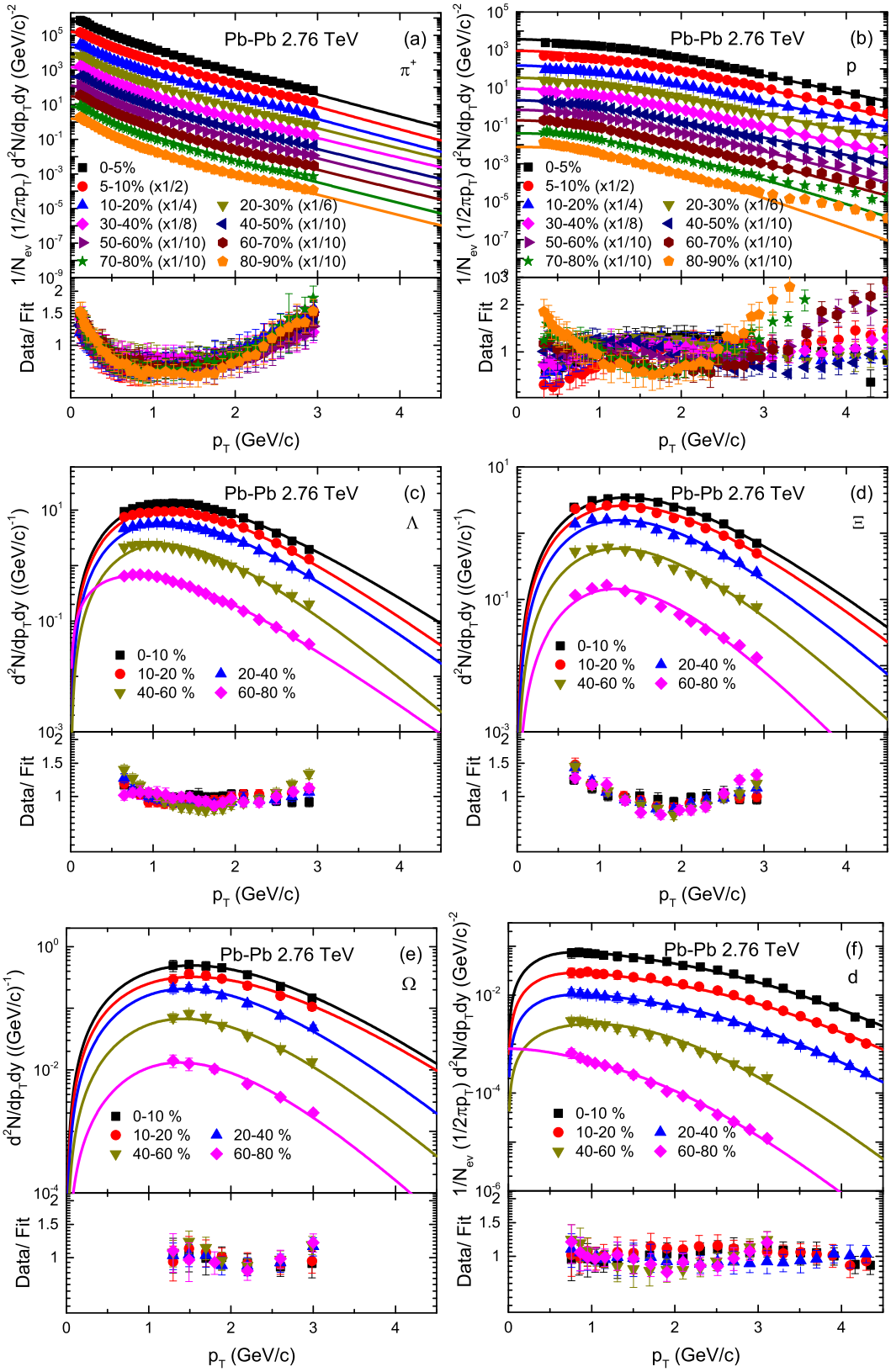

Fig. 2. Transverse momentum spectra of π^+, p, Λ, Ξ, Ω rapidity and deuteron (d) produced in different centrality intervals in Pb-Pb collisions at 2.76 TeV. Different symbols represent the p_T spectra of different particles measured by the ALICE collaboration [58–60] and the curves are our fitted results with BGBW model. The corresponding results of data/fit is presented in each panel.

Preprints (www.preprints.org) | NOT PEER-REVIEWED | Posted: 8 April 2021 doi:10.20944/preprints202104.0246.v1

20–30%, 30–40%, 40–50%, 50–60%, 60–70% and 70–80% p are scaled by 1/3, 1/7, 1/26, 1/60, 1/150, 1/250, 1/400 and 1/600 respectively.

Figure 2 is similar to Fig.1 but it shows the the p_T spectra of π^+, p, Λ, Ξ, Ω and deuteron (d) in different centrality intervals in Pb-Pb collisions at 2.76 TeV. The spectra is distributed in different centrality intervals, e:g for π^+, and p 0–5%, 5–10%, 10–20%, 20–30%, 30–40%, 40–50%, 50–60%, 60–70% 70–80% and 80–90% at $|y| < 0.5$, for Λ, Ξ, and Ω 0–10%, 10–20%, 20–40%, 40–60%, and 60–80%, for Ω, 0–10%, 10–20%, 20–40%, 40–60% and 60–80% at $y = 0$, and for deuteron (d) 0–10%, 10–20%, 20–40%, 40–60% and 60–80%, at $|y| < 0.5$. The spectra of of π^+ and p in 5–10%, 10–20%, 20–30%, 30–40%, 40–50%, 50–60%, 60–70% and 70–80% centrality intervals are scaled with 1/2, 1/4, 1/6, 1/8, 1/10, 1/10, 1/10, 1/10 and 1/10 respectively. The symbols are cited from the experimental data measured by the ALICE Collaboration at Large Hadron Collider (LHC) [58–60]. In the figure, the curves are our fitted results with Eq. (1). The corresponding values of free parameters (T_0, V, β_T and n_0), normalization constant (N_0), χ^2 and number of degree of freedom (ndof) are listed in Table 1 in which the parameter trend will be analyzed and discussed below. One can see that the p_T spectra of the particles are shown to obey approximately the blast wave model with boltzmann Gibbs statistics.

Figure 3 analyze the dependence of kinetic freezeout temperature (T_0) on centrality class (C%) and mass of the particles. Panel (a) and (b) shows the result for Au-Au and Pb-Pb collisions respectively. The colored symbols represent different species of particles and the particles from left to right shows the result of T_0 from central to peripheral collisions. One can see that the kinetic freezeout temperature of the emission source decreases with the decrease of centrality from central to peripheral collisions. The central collision corresponds to very violent collision due to large number of participant nucleons that makes the degree of excitation of system high and results in high temperature, but as the centrality decreases, the collision become less and less violent due to less and less number of particles in the interaction which results in decreasing the degree of excitation of they system and correspondingly the temperature decrease more and more. This result is consistent with [5, 6, 18, 27, 28, 29, 61] but inconsistent with [62–66]. In addition, the dependence of T_0 on m_0 is not clear. The pion and proton has almost same values for T_0 and similarly the the strange (muti-strange) particles. Deuteron has the largest mass and it freezeout at the same time with pion and proton. The reason maybe the production cross-section of the interacting particle. According to kinematics, the reactions with lower cross-section is supposed to be switched-off at higher temperatures/densities or earlier in time than the reactions with higher cross-sections. π^+, p and d are non-strange particles, so they have the same T_0, while Λ, $\Xi(\bar{\Xi}^+)$ and $\Omega(\bar{\Omega}^+)$ are strange flavored particles, so they have the same T_0. The non-strange particles has larger production cross-section than the strange or multi-strange particles, therefore the non-strange particles freezeout later than the strange (multi)strange particles. This results is consistent with one of our recent work [10], however ref.[10] observed separate decoupling of strange and multi-strange also. It is noteworthy that the observed T_0 at RHIC is lower than that of LHC.

Figure 4 is similar to Fig.3, but shows the dependence of transverse flow velocity (β_T) on centrality class and mass of the particles. One can see that β_T depends on the rest mass of the particles. Greater the mass of the particle is, smaller the transverse flow velocity which is a natural hydrodynamical behavior [67]. Furthermore, there is no centrality dependence of β_T observed in present work, as β_T is almost the same at the central and peripheral collisions. However β_T is larger at LHC than that of RHIC.

Figure 5 is similar to Fig.3 and 4, but shows the dependence of V on centrality class and mass of the particles. One can see that V decrease continuously from central to peripheral collisions because the central collisions correspond to large number of binary collisions due to the re-scattering of partons and hence the system with more participants reaches quickly to equilibrium state. While the number of participants decrease with the decrease of event centrality and the system goes to equilibrium state in a steady manner

Preprints (www.preprints.org) | NOT PEER-REVIEWED | Posted: 8 April 2021 doi:10.20944/preprints202104.0246.v1

Table 1. Values of free parameters T_0 and β_T, V and normalization constant (N_0), n_0, χ^2, and degree of freedom (dof) corresponding to the curves in Figs. 1–6.

Collisions	Centrality	Particle	T_0 (GeV)	β_T (c)	$V(fm^3)$	N_0	n_0	χ^2/dof
Fig. 1	$0-5\%$	π^+	0.111 ± 0.005	0.520 ± 0.008	5000 ± 193	0.25 ± 0.06	0.8	3/5
Au-Au	$5-10\%$	–	0.107 ± 0.004	0.518 ± 0.008	4800 ± 170	0.24 ± 0.004	1.3	7/5
62.4 GeV	$10-20\%$	–	0.103 ± 0.005	0.520 ± 0.009	4615 ± 165	0.185 ± 0.004	2.6	2/5
	$20-30\%$	–	0.098 ± 0.006	0.515 ± 0.011	4430 ± 161	0.136 ± 0.0005	1.3	2/5
	$30-40\%$	–	0.095 ± 0.004	0.517 ± 0.009	4250 ± 160	0.0975 ± 0.004	1.2	2/5
	$40-50\%$	–	0.090 ± 0.006	0.512 ± 0.010	4000 ± 150	0.067 ± 0.004	1.8	5/5
	$50-60\%$	–	0.086 ± 0.005	0.514 ± 0.010	3800 ± 150	0.049 ± 0.005	2	7/5
	$60-70\%$	–	0.081 ± 0.005	0.513 ± 0.011	3610 ± 170	0.029 ± 0.004	2	1/5
	$70-80\%$	–	0.080 ± 0.004	0.510 ± 0.007	3400 ± 176	0.015 ± 0.005	2	4/5
Fig. 1	$0-5\%$	p	0.113 ± 0.006	0.490 ± 0.010	4700 ± 170	0.0165 ± 0.003	1.2	33/9
Au-Au	$5-10\%$	–	0.109 ± 0.005	0.500 ± 0.011	4530 ± 160	0.0094 ± 0.0005	1	20/9
62.4 GeV	$10-20\%$	–	0.105 ± 0.004	0.500 ± 0.009	4400 ± 155	0.0113 ± 0.004	1.2	5/9
	$20-30\%$	–	0.100 ± 0.005	0.490 ± 0.010	4225 ± 140	0.008 ± 0.0005	1.3	3/9
	$30-40\%$	–	0.097 ± 0.005	0.488 ± 0.011	4160 ± 150	0.0055 ± 0.0004	1.5	7/9
	$40-50\%$	–	0.093 ± 0.005	0.489 ± 0.009	3900 ± 150	0.0035 ± 0.0004	0.8	3/9
	$50-60\%$	–	0.088 ± 0.004	0.487 ± 0.011	3700 ± 158	0.0022 ± 0.0003	0.6	4/9
	$60-70\%$	–	0.083 ± 0.006	0.480 ± 0.012	3530 ± 160	0.00175 ± 0.0004	0.3	4/9
	$70-80\%$	–	0.081 ± 0.005	0.481 ± 0.009	3310 ± 130	0.00055 ± 0.00005	0.4	14/9
Fig. 1	$0-5\%$	Λ	0.137 ± 0.006	0.470 ± 0.009	4300 ± 152	0.023 ± 0.004	0.7	1/7
Au-Au	$5-10\%$	–	0.133 ± 0.005	0.468 ± 0.010	4120 ± 160	0.002 ± 0.0004	0.7	1/7
62.4 GeV	$10-20\%$	–	0.130 ± 0.006	0.470 ± 0.011	4000 ± 187	0.00017 ± 0.00004	0.7	1/7
	$20-30\%$	–	0.126 ± 0.004	0.465 ± 0.010	3830 ± 164	$1 \times 10^{-5} \pm 4 \times 10^{-6}$	0.8	1/7
	$30-40\%$	–	0.123 ± 0.004	0.467 ± 0.012	3650 ± 160	$9 \times 10^{-7} \pm 5 \times 10^{-8}$	0.8	1/7
	$40-60\%$	–	0.120 ± 0.005	0.460 ± 0.011	3400 ± 156	$4 \times 10^{-8} \pm 3 \times 10^{-9}$	0.8	5/7
	$60-80\%$	–	0.117 ± 0.005	0.460 ± 0.012	3200 ± 140	$1 \times 10^{-9} \pm 5 \times 10^{-10}$	0.9	5/7
Fig. 1	$0-5\%$	$\bar{\Xi}^+$	0.138 ± 0.004	0.455 ± 0.011	4150 ± 150	0.0008 ± 0.00004	0.7	0.4/5
Au-Au	$5-10\%$	–	0.134 ± 0.005	0.450 ± 0.011	4000 ± 140	$6.5 \times 10^{-5} \pm 6 \times 10^{-6}$	1	3/6
62.4 GeV	$10-20\%$	–	0.131 ± 0.006	0.452 ± 0.012	3800 ± 157	$5.2 \times 10^{-6} \pm 4 \times 10^{-7}$	0.8	2/6
	$20-40\%$	–	0.127 ± 0.004	0.450 ± 0.010	3600 ± 148	$4.5 \times 10^{-7} \pm 6 \times 10^{-8}$	0.7	3/6
	$40-60\%$	–	0.124 ± 0.005	0.453 ± 0.010	3400 ± 150	$8.8 \times 10^{-9} \pm 5 \times 10^{-10}$	0.7	1/6
	$60-80\%$	–	0.120 ± 0.005	0.450 ± 0.009	3200 ± 146	$3.4 \times 10^{-10} \pm 5 \times 10^{-11}$	0.4	3/4
Fig. 1	$0-20\%$	$\bar{\Omega}^+$	0.138 ± 0.004	0.440 ± 0.008	4000 ± 155	$5.2 \times 10^{-5} \pm 5 \times 10^{-6}$	0.6	0.3/0
Au-Au	$20-40\%$	–	0.134 ± 0.006	0.435 ± 0.011	3800 ± 146	$2 \times 10^{-7} \pm 6 \times 10^{-8}$	1	1/0
62.4 GeV	$40-60\%$	–	0.127 ± 0.005	0.436 ± 0.012	3600 ± 160	$3.2 \times 10^{-9} \pm 7 \times 10^{-10}$	0.7	2/-1
Fig. 1	$0-10\%$	d	0.114 ± 0.005	0.400 ± 0.011	3400 ± 140	0.00085 ± 0.00005	1.6	3/7
Au-Au	$10-20\%$	–	0.109 ± 0.006	0.395 ± 0.010	3200 ± 150	0.00034 ± 0.00004	1.6	2/7
62.4 GeV	$20-40\%$	–	0.104 ± 0.005	0.396 ± 0.011	3000 ± 145	0.0001 ± 0.00004	1.5	1/7
	$40-60\%$	–	0.097 ± 0.005	0.393 ± 0.012	2800 ± 170	$2 \times 10^{-5} \pm 5 \times 10^{-6}$	1.3	1/7
	$60-80\%$	–	0.090 ± 0.004	0.392 ± 0.011	2632 ± 150	$2 \times 10^{-6} \pm 4 \times 10^{-7}$	0.9	22/6
Fig. 2	$0-5\%$	π^+	0.130 ± 0.005	0.584 ± 0.012	7000 ± 200	345 ± 36	0.8	89/36
Pb-Pb	$5-10\%$	–	0.127 ± 0.006	0.583 ± 0.010	6816 ± 191	165.55 ± 23	0.7	158/36
2.76 TeV	$10-20\%$	–	0.123 ± 0.004	0.580 ± 0.011	6650 ± 185	60.55 ± 8	0.8	93/36
	$20-30\%$	–	0.119 ± 0.005	0.581 ± 0.010	6392 ± 180	18.80 ± 3	0.9	58/36
	$30-40\%$	–	0.115 ± 0.005	0.580 ± 0.012	6200 ± 185	6.3 ± 0.4	1	54/36
	$40-50\%$	–	0.112 ± 0.006	0.580 ± 0.011	6000 ± 170	2.2 ± 0.3	1	92/36
	$50-60\%$	–	0.109 ± 0.004	0.581 ± 0.011	5843 ± 162	0.66 ± 0.04	1	100/36
	$60-70\%$	–	0.106 ± 0.006	0.579 ± 0.010	5670 ± 170	0.16 ± 0.03	1.1	197/36
	$70-80\%$	–	0.101 ± 0.005	0.578 ± 0.011	5500 ± 166	0.04 ± 0.005	1.1	151/36
	$80-90\%$	–	0.098 ± 0.004	0.576 ± 0.010	5300 ± 160	0.008 ± 0.0004	1.1	221/36
Fig. 2	$0-5\%$	p	0.131 ± 0.005	0.570 ± 0.010	6700 ± 180	8 ± 0.7	1	58/30
Pb-Pb	$5-10\%$	–	0.127 ± 0.006	0.570 ± 0.010	6500 ± 170	4.05 ± 0.5	0.9	125/37
2.76 TeV	$10-20\%$	–	0.123 ± 0.005	0.570 ± 0.009	6320 ± 170	1.35 ± 0.3	1.1	37/33
	$20-30\%$	–	0.120 ± 0.006	0.570 ± 0.011	6180 ± 160	0.9 ± 0.05	1.1	34/31
	$30-40\%$	–	0.116 ± 0.005	0.565 ± 0.012	6000 ± 180	0.16 ± 0.04	1.07	17/31
	$40-50\%$	–	0.112 ± 0.006	0.567 ± 0.009	5830 ± 170	0.05 ± 0.004	1.1	108/33
	$50-60\%$	–	0.108 ± 0.005	0.564 ± 0.010	5650 ± 165	0.016 ± 0.003	1	62/31
	$60-70\%$	–	0.104 ± 0.005	0.562 ± 0.011	5480 ± 170	0.0045 ± 0.0004	1	140/34
	$70-80\%$	–	0.101 ± 0.005	0.562 ± 0.009	5300 ± 180	0.001 ± 0.0003	0.9	214/36
	$80-90\%$	–	0.097 ± 0.004	0.560 ± 0.010	5100 ± 180	0.0002 ± 0.00003	0.8	207/37

Preprints (www.preprints.org) | NOT PEER-REVIEWED | Posted: 8 April 2021 doi:10.20944/preprints202104.0246.v1

Fig. 2	$0-10\%$	Λ	0.155 ± 0.005	0.500 ± 0.011	6000 ± 200	0.13 ± 0.03	0.9	28/14
Pb-Pb	$10-20\%$	–	0.152 ± 0.006	0.497 ± 0.009	5800 ± 180	0.1 ± 0.03	0.8	27/14
2.76 TeV	$20-40\%$	–	0.147 ± 0.004	0.496 ± 0.010	5600 ± 180	0.06 ± 0.004	0.8	35/14
	$40-60\%$	–	0.142 ± 0.005	0.495 ± 0.011	5400 ± 185	0.024 ± 0.004	0.6	124/14
	$60-80\%$	–	0.137 ± 0.005	0.494 ± 0.010	5200 ± 170	0.0074 ± 0.0005	1.1	17/14
Fig. 2	$0-10\%$	Ξ	0.156 ± 0.006	0.480 ± 0.010	5500 ± 200	0.0180 ± 0.004	1	16/7
Pb-Pb	$10-20\%$	–	0.152 ± 0.005	0.477 ± 0.012	5300 ± 180	0.0140 ± 0.003	1	37/7
2.76 TeV	$20-40\%$	–	0.148 ± 0.005	0.474 ± 0.010	5126 ± 170	0.0085 ± 40.0005	0.9	63/7
	$40-60\%$	–	0.144 ± 0.005	0.473 ± 0.009	4950 ± 160	0.0032 ± 0.0005	0.8	82/7
	$60-80\%$	–	0.140 ± 0.006	0.470 ± 0.012	4700 ± 180	0.0008 ± 0.00005	0.6	107/7
Fig. 2	$0-10\%$	Ω	0.158 ± 0.005	0.460 ± 0.010	5000 ± 150	0.0014 ± 0.0003	1.1	12/2
Pb-Pb	$10-20\%$	–	0.154 ± 0.005	0.458 ± 0.009	4817 ± 160	$9.7 \times 10^{-4} \pm 4 \times 10^{-5}$	1.2	1/2
2.76 TeV	$20-40\%$	–	0.150 ± 0.004	0.457 ± 0.012	4600 ± 180	$6 \times 10^{-4} \pm 6 \times 10^{-5}$	0.9	3/2
	$40-60\%$	–	0.147 ± 0.005	0.456 ± 0.010	4400 ± 120	$2 \times 10^{-4} \pm 5 \times 10^{-5}$	0.8	6/2
	$60-80\%$	–	0.143 ± 0.004	0.453 ± 0.012	4200 ± 180	$4 \times 10^{-5} \pm 5 \times 10^{-6}$	0.7	5/1
Fig. 2	$0-10\%$	d	0.133 ± 0.005	0.430 ± 0.008	4500 ± 170	$4.6 \times 10^{-4} \pm 5 \times 10^{-5}$	1.8	6/16
Pb-Pb	$10-20\%$	–	0.130 ± 0.005	0.428 ± 0.011	4300 ± 160	$1.8 \times 10^{-4} 4 \pm \times 10^{-5}$	1.8	6/16
2.76 TeV	$20-40\%$	–	0.126 ± 0.006	0.426 ± 0.009	4100 ± 153	$6.6 \times 10^{-5} \pm 4 \times 10^{-6}$	1.7	4/16
	$40-60\%$	–	0.122 ± 0.004	0.423 ± 0.011	3938 ± 160	$1.5 \times 10^{-5} \pm 5 \times 10^{-6}$	1.2	15/10
	$60-80\%$	–	0.118 ± 0.005	0.422 ± 0.012	3650 ± 150	$2.8 \times 10^{-6} \pm 4 \times 10^{-7}$	1.3	10/10

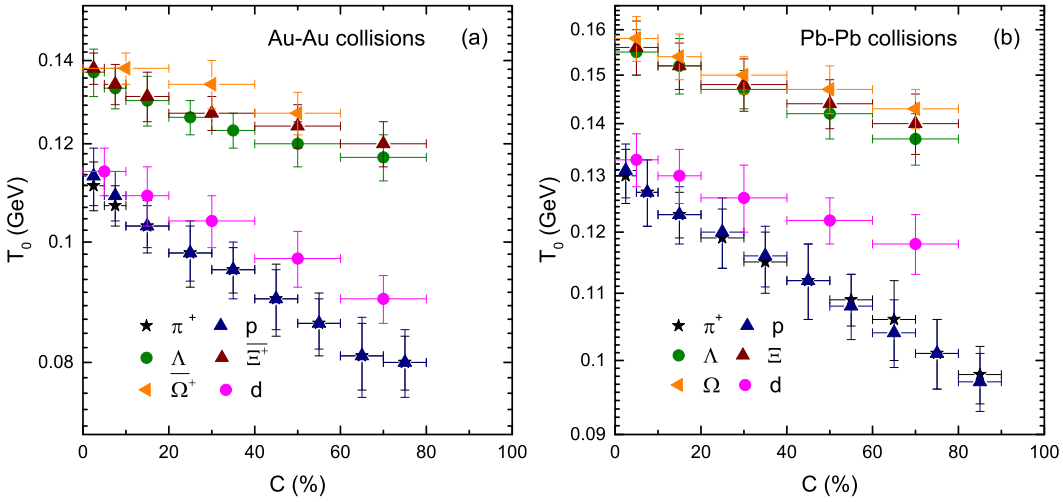

Fig. 3. Dependence of T_0 on centrality class ($C\%$) and rest mass (m_0) of the particle.

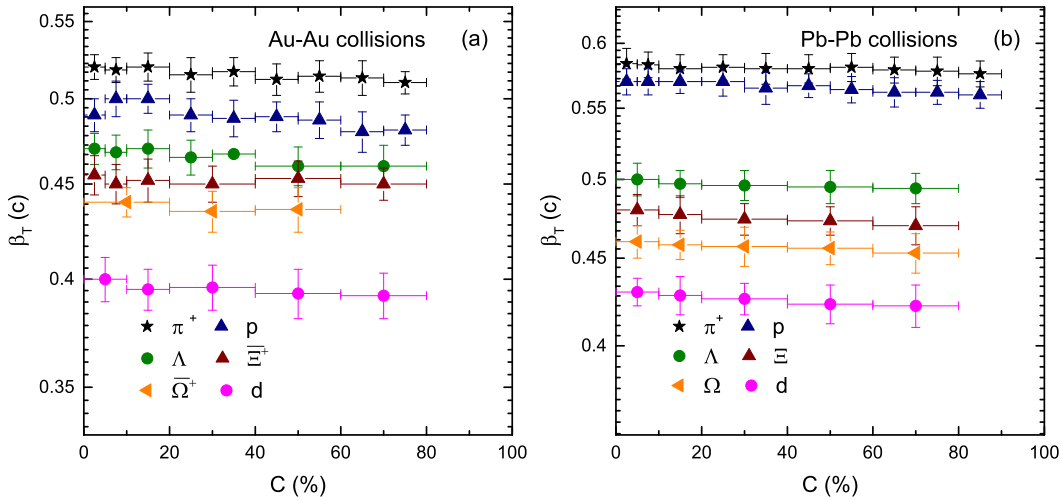

Fig. 4. Dependence of β_T on centrality class ($C\%$) and rest mass (m_0) of the particle.

Preprints (www.preprints.org) | NOT PEER-REVIEWED | Posted: 8 April 2021 doi:10.20944/preprints202104.0246.v1

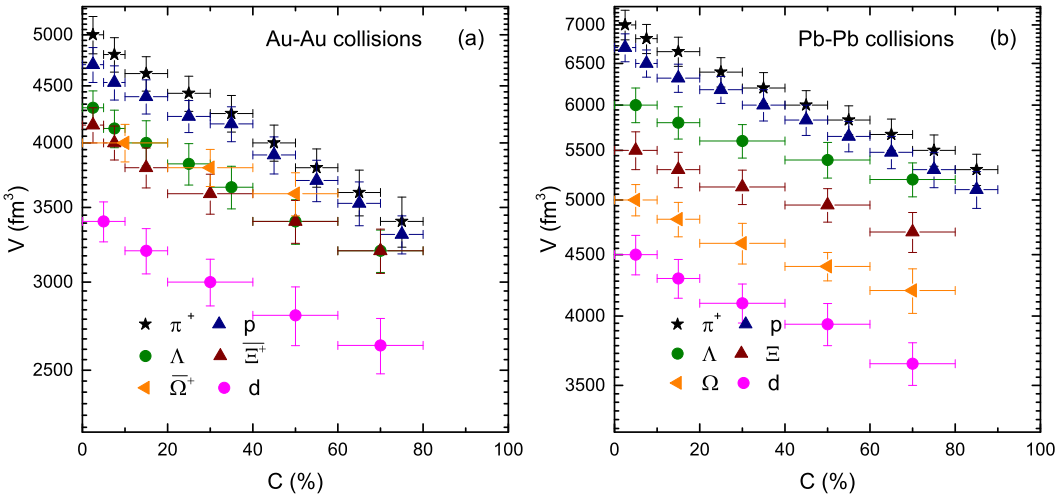

Fig. 5. Dependence of V on centrality class (C%) and rest mass (m_0) of the particle.

from central to peripheral collisions. Additionally, V depends on the mass of the particles. Greater the mass of the particle is, lower the V. V at LHC is larger than that at RHIC.

4. Conclusions

The main observations and conclusions are summarized here.

a) The transverse momentum spectra of different particle species are analyzed by the blast wave model with Boltzmann Gibbs statistics and the bulk properties in terms of the kinetic freezeout temperature, transverse flow velocity and freezeout volume are extracted in different centrality classes in Au-Au and Pb-Pb collisions at 62.4 GeV and 2.76 TeV respectively.

b) It is observed that T_0 is dependent on the cross-section of the interacting particle, i:e Larger the production cross-section of the interacting particle correspond to smaller T_0.

c) A double kinetic freezeout scenario is observed due to the separate decoupling of non-strange and strange (strange) particles.

d) The transverse flow velocity (β_T) and kinetic freezeout volume (V) are observed to depend on the mass of the particles, i:e. Larger the mass of the particle correspond to smaller β_T and V.

e) Kinetic freezeout temperature (T_0) and freezeout volume (V) decrease from central peripheral collisions due to decrease of degree of excitation of interacting system and the decrease of the number of binary collisions due to the re-scattering of partons respectively from central to peripheral collisions. While β_T is observed to be independent of centrality and remians almost unchanged from central to peripheral collisions.

f) T_0, β_T and V are observed to be larger at LHC collisions that at RHIC.)

Author Contributions: The authors contributed to the paper in this way: conceptualization, M. Waqas; methodology, M. Waqas and G.X.Peng.; software, M. Waqas.; validation, M. Waqas and G.X.Peng; formal analysis, M. Waqas; investigation, M. Waqas; resources, G.X.Peng; data curation, M. Waqas; writing C original draft preparation, M. Waqas; writing C review and editing, M. Waqas; visualization, M. Waqas; supervision, G.X.Peng; project administration, G.X.Peng; funding acquisition, G.X.Peng

Institutional Review Board Statement: The authors declare that they are in compliance with ethical standards regarding the content of this paper.

Data Availability Statement: The data used to support the findings of this study are included within the article and are cited at relevant places within the text as references.

Acknowledgments: The authors would like to thank support from the National Natural Science Foundation of China (Grant Nos. 11875052, 11575190, and 11135011).

References

1. Cleymans J, Oeschler. H, Redlich. K and Wheaton. S, "Comparison of chemical freeze-out criteria in heavy-ion collisions," Phys. Rev. C **2006**, 73, 034905 doi:10.1103/PhysRevC.73.034905 [arXiv:hep-ph/0511094 [hep-ph]].
2. Andronic. A, Braun-Munzinger. P and Stachel. J, "Hadron production in central nucleus-nucleus collisions at chemical freeze-out," Nucl. Phys. A **2006**, 772, 167-199 doi:10.1016/j.nuclphysa.2006.03.012 [arXiv:nucl-th/0511071 [nucl-th]].
3. Andronic. A, Braun-Munzinger. P and Stachel. J, "The Horn, the hadron mass spectrum and the QCD phase diagram: The Statistical model of hadron production in central nucleus-nucleus collisions," Nucl. Phys. A **2010**, 834, 237C-240C doi:10.1016/j.nuclphysa.2009.12.048 [arXiv:0911.4931 [nucl-th]].
4. Andronic. A, Braun-Munzinger. P and Stachel. J, "Thermal hadron production in relativistic nuclear collisions," Acta Phys. Polon. B **2009**, 40, 1005-1012 [arXiv:0901.2909 [nucl-th]].
5. Waqas. M, Liu. F-H, Fakhraddin. S and Rahim. M. A, "Possible scenarios for single, double, or multiple kinetic freeze-out in high energy collisions," Indian J. Phys. **2019**, 93, 1329-1343 doi:10.1007/s12648-019-01396-9 [arXiv:1806.04312 [nucl-th]].
6. Waqas. M, and Li. B. C "Kinetic freeze-out temperature and transverse flow velocity in Au-Au collisions at RHIC-BES energies," Adv. High Energ Phys. **2020**, 2020, 1787183. [arXiv:1909.11339 [hep-ph]].
7. Khuntia. A, Sharma. H, Kumar Tiwari. S, Sahoo. R and Cleymans. J, Eur. Phys. J. A **2019**, 55 , 3 doi:10.1140/epja/i2019-12669-6 [arXiv:1808.02383 [hep-ph]].
8. Thakur. D, Tripathy. S, Garg. P, Sahoo. R and Cleymans. J, Acta Phys. Polon. Supp. **2016**, 9, 329 doi:10.5506/APhysPolBSupp.9.329 [arXiv:1603.04971 [hep-ph]].
9. Shao. M, Yi. L, Tang. Z, Chen. H, Li. C and Xu. Z, J. Phys. G **2010**, 37, 085104 doi:10.1088/0954-3899/37/8/085104 [arXiv:0912.0993 [nucl-ex]].
10. Waqas. M, Peng. G. X and Liu. F-H "An evidence of triple kinetic freezeout scenario observed in all centrality intervals in Cu-Cu, Au-Au and Pb-Pb collisions at high energies," doi:10.1088/1361-6471 [arXiv:2101.07971 [hep-ph]].
11. Abelev. B *et al.* [ALICE], "Pion, Kaon, and Proton Production in Central Pb–Pb Collisions at $\sqrt{s_{NN}} = 2.76$ TeV," Phys. Rev. Lett. **2012** 109, 252301 doi:10.1103/PhysRevLett.109.252301 [arXiv:1208.1974 [hep-ex]].
12. Andronic. A, "An overview of the experimental study of quark-gluon matter in high-energy nucleus-nucleus collisions," Int. J. Mod. Phys. A **2014**, 29, 1430047 doi:10.1142/S0217751X14300476 [arXiv:1407.5003 [nucl-ex]].
13. Zhang. S, Ma. Y. G, Chen.J . H and Zhong. C, "Production of Kaon and Λ in Nucleus-Nucleus Collisions at Ultrarelativistic Energy from a Blast-Wave Model," Adv. High Energy Phys. **2015**, 2015, 460590 doi:10.1155/2015/460590 [arXiv:1411.1500 [nucl-th]].
14. Zhang. S, Ma. Y. G, Chen.J . H and Zhong. C, "Beam energy dependence of Hanbury-Brown-Twiss radii from a blast-wave model," Adv. High Energy Phys. **2016**, 2016, 9414239 doi:10.1155/2016/9414239 [arXiv:1602.01564 [nucl-th]].
15. Waqas. M, Liu. F-H, Li. L. L and Alfanda. H. M "Effective (kinetic freeze-out) temperature, transverse flow velocity and kinetic freeze-out volume in high energy collisions," Nucl. Sci. Tech. **2010**, 31, 109 doi:10.1007/s41365-020-00821-7 [arXiv:2001.06796 [hep-ph]].
16. Waqas. M, Liu. F-H, and Wazir. Z, "Dependence of temperatures and kinetic freeze-out volume on centrality in Au-Au and Pb-Pb collisions at high energy," Adv. High Energy Phys. **2020**, 2020, 8198126 doi:10.1155/2020/8198126 [arXiv:2004.03773 [hep-ph]].
17. Waqas. M, Liu. F-H, "Centrality dependence of kinetic freeze-out temperature and transverse flow velocity in high energy nuclear collisions," [arXiv:1806.05863 [hep-ph]].
18. Wang. Q and Liu. F-H, "Initial and final state temperatures of antiproton emission sources in high energy collisions," Int. J. Theor. Phys. **2019**, 58, 4119-4138 doi:10.1007/s10773-019-04278-2 [arXiv:1909.02390 [hep-ph]].
19. Schnedermann. E, Sollfrank. J and Heinz. U. W "Thermal phenomenology of hadrons from 200-A/GeV S+S collisions," Phys. Rev. C **1993**, 48, 2462-2475 doi:10.1103/PhysRevC.48.2462 [arXiv:nucl-th/9307020 [nucl-th]].
20. Abelev. B. I *et al.* [STAR], "Identified particle production, azimuthal anisotropy, and interferometry measurements in Au+Au collisions at s(NN)**(1/2) = 9.2- GeV," Phys. Rev. C **2010**, 81, 024911 doi:10.1103/PhysRevC.81.024911 [arXiv:0909.4131 [nucl-ex]].
21. Abelev. B. I *et al.* [STAR], Phys. Rev. C **2009**, 79, 034909 doi:10.1103/PhysRevC.79.034909 [arXiv:0808.2041 [nucl-ex]].
22. Tang. Z, Yi. L, Ruan. L, Shao. M, Chen. H, Li. C, Mohanty. B, Sorensen. P, Tang. A and Xu. Z, Chin. Phys. Lett. **2013**, 30, 031201 doi:10.1088/0256-307X/30/3/031201 [arXiv:1101.1912 [nucl-ex]].
23. Jiang. K, Zhu. Y, Liu. W, Chen. H, Li. C, Ruan. L, Tang. Z, and Z. Xu, Phys. Rev. C **2015**, 91, 024910 doi:10.1103/PhysRevC.91.024910 [arXiv:1312.4230 [nucl-ex]]
24. Tang. Z, Xu. Y, Ruan. L, van Buren. G, Wang. F and Xu. Z, Phys. Rev. C **2009**, 79, 051901 doi:10.1103/PhysRevC.79.051901 [arXiv:0812.1609 [nucl-ex]].
25. Wei. H. R, Liu. F-H and Lacey. R. A, Eur. Phys. J. A **2016**, 52, 102 doi:10.1140/epja/i2016-16102-6 [arXiv:1601.07045 [hep-ph]].
26. Wei. H. R, Liu. F-H and Lacey. R. A, J. Phys. G **2016**, 43, 125102 doi:10.1088/0954-3899/43/12/125102 [arXiv:1509.09083 [nucl-ex]].
27. Lao H.-L, Wei. H. R, Liu F-H and Lacey. R. A, Eur. Phys. J. A **2016**, 52, 203 doi:10.1140/epja/i2016-16203-2 [arXiv:1601.00045 [nucl-th]].
28. Lao H.-L, Liu F-H, Li B. C., Duan M. Y and Lacey R. A Nucl. Sci. Tech. **2018**, 29, 164 doi:10.1007/s41365-018-0504-z [arXiv:1708.07749 [nucl-th]].

29. Lao H.-L, Liu F-H, Li B. C., and Duan M. Y Nucl. Sci. Tech. **2018**, 29, 82 doi:10.1007/s41365-018-0425-x [arXiv:1703.04944 [nucl-th]].
30. Zheng. H and Zhu. L, Adv. High Energy Phys. **2016**, 2016, 9632126 doi:10.1155/2016/9632126 [arXiv:1512.03555 [nucl-th]].
31. Cleymans. J and Worku. D, Eur. Phys. J. A **2012**, 48, 160 doi:10.1140/epja/i2012-12160-0 [arXiv:1203.4343 [hep-ph]].
32. Takeuchi. S, Murase. K, Hirano. T, Huovinen. P and Nara. Y, Phys. Rev. C **2015**, 92, 044907 doi:10.1103/PhysRevC.92.044907 [arXiv:1505.05961 [nucl-th]].
33. Heinz U. W, Hydrodynamics at RHIC: how well does it work, where and how does it break down?,Journal of Physics G: Nuclear and Particle Physics, **2005**, 31, S717. doi: 10.1088/0954-3899/31/6/012, [arXiv:nucl-th/0412094]
34. Heiselberg H. and Levy A.-M, Elliptic flow and HanburyBrownCTwiss correlations in noncentral nuclear collisions,Physical Review C. **1999**, 59, 2716C2727,
35. Russo R, [arXiv:1511.04380 [nucl-ex]].
36. Bíró G, Barnaföldi G. G, Biró T. S, Ürmössy K and Takács Á., Entropy **2017**, 19, 88 doi:10.3390/e19030088 [arXiv:1702.02842 [hep-ph]].
37. Sadhu. S and Ghosh. P, Phys. Rev. D **2019**, 99, 034020 doi:10.1103/PhysRevD.99.034020 [arXiv:1901.06787 [hep-ph]].
38. Chatrchyan. S *et al.* [CMS], Eur. Phys. J. C **2012**, 72, 1945 doi:10.1140/epjc/s10052-012-1945-x [arXiv:1202.2554 [nucl-ex]].
39. Tsallis. C, J. Statist. Phys. **1988**, 52, 479-487 doi:10.1007/BF01016429
40. Abelev B. I, Adams J, Aggarwal M. M et al., Strange particle production in p + p collisions at 200 GeV,Physical Review C. **2007**, 75, 064901
41. Petrovici. M, Andrei C, Berceanu I, Bercuci A, Herghelegiu A and Pop A, AIP Conf. Proc. **2015**, 1645, 52-60 doi:10.1063/1.4909559. [arXiv:1411.0869 [nucl-ex]].
42. Hagedorn R, Multiplicities, p_T distributions and the expected hadron quark-gluon phase transition,La Rivista del Nuovo Cimento **1983**, 6, 1C50
43. Suleymanov M, Int. J. Mod. Phys. E **2018**, 27, 1850008 doi:10.1142/S0218301318500088 [arXiv:1707.03420 [nucl-ex]].
44. Abelev B. B *et al.* [ALICE], Eur. Phys. J. C **2015**, 75, 1 doi:10.1140/epjc/s10052-014-3191-x [arXiv:1406.3206 [nucl-ex]].
45. Odorico R, Phys. Lett. B **1982**, 118, 151-154 doi:10.1016/0370-2693(82)90620-7
46. Arnison G, Astbury A, Aubert B et al., Transverse momentum spectra for charged particles at the CERN protonantiproton collider,Physics Letters B **1982**, 118, 167C172
47. Biyajima M, Mizoguchi T and Suzuki N, Int. J. Mod. Phys. A **2017**, 32, 1750057 doi:10.1142/S0217751X17500579 [arXiv:1604.01264 [hep-ph]].
48. Abelev B *et al.* [ALICE], Phys. Lett. B **2012**, 708, 265-275 doi:10.1016/j.physletb.2012.01.063 [arXiv:1201.3791 [hep-ex]].
49. Lakomov I [ALICE], Nucl. Phys. A **2014**, 931, 1179-1183 doi:10.1016/j.nuclphysa.2014.08.062 [arXiv:1408.0702 [hep-ex]].
50. Abelev B *et al.* [ALICE], Phys. Lett. B **2012**, 718, 295-306 [erratum: Phys. Lett. B **748** (2015), 472-473] doi:10.1016/j.physletb.2012.10.078 [arXiv:1203.3641 [hep-ex]].
51. Abelev B *et al.* [ALICE], Phys. Lett. B **2012**, 710, 557-568 doi:10.1016/j.physletb.2012.03.038 [arXiv:1112.2222 [nucl-ex]].
52. Abt I *et al.* [HERA-B], Eur. Phys. J. C **2007**, 50, 315-328 doi:10.1140/epjc/s10052-007-0237-3 [arXiv:hep-ex/0606049 [hep-ex]]
53. De Falco A [ALICE], J. Phys. G **2011**, 38, 124083 doi:10.1088/0954-3899/38/12/124083 [arXiv:1106.4140 [nucl-ex]].
54. Aamodt K *et al.* [ALICE], Phys. Lett. B **2010**, 693, 53-68 doi:10.1016/j.physletb.2010.08.026 [arXiv:1007.0719 [hep-ex]].
55. Abelev B. I *et al.* [STAR], Phys. Rev. C **2009**, 79, 034909 doi:10.1103/PhysRevC.79.034909 [arXiv:0808.2041 [nucl-ex]].
56. Aggarwal M. M *et al.* [STAR], Phys. Rev. C **2011**, 83, 024901 doi:10.1103/PhysRevC.83.024901 [arXiv:1010.0142 [nucl-ex]]
57. Adam J *et al.* [STAR], Phys. Rev. C **2019**, 99, 064905 doi:10.1103/PhysRevC.99.064905 [arXiv:1903.11778 [nucl-ex]].
58. Abelev B *et al.* [ALICE], Phys. Rev. C **2013**, 88, 044910 doi:10.1103/PhysRevC.88.044910 [arXiv:1303.0737 [hep-ex]].
59. Begun V, Florkowski W and Rybczynski M, Phys. Rev. C **2014**, 90, (2014), 054912 doi:10.1103/PhysRevC.90.054912 [arXiv:1405.7252 [hep-ph]].
60. Adam J *et al.* [ALICE], Phys. Rev. C **2016**, 93, 024917 doi:10.1103/PhysRevC.93.024917 [arXiv:1506.08951 [nucl-ex]].
61. Waqas M and Liu F-H, Eur. Phys. J. Plus **2020**, 135, 147 doi:10.1140/epjp/s13360-020-00213-1 [arXiv:1911.01709 [hep-ph]].
62. Che G. R, Gu J. B, Zhang W. C and Zheng H, [arXiv:2010.14880 [nucl-th]].
63. Bashir I. u and Uddin S, Commun. Theor. Phys. **2017**, 68, 500 doi:10.1088/0253-6102/68/4/500 [arXiv:1510.05874 [hep-ph]].
64. Uddin S, Bhat R. A and Bashir I. u, [arXiv:1412.2663 [hep-ph]].
65. Waqas M and Peng G. X, [arXiv:2103.07852 [hep-ph]].
66. Acharya S *et al.* [ALICE], Phys. Rev. C **2020**, 101, 044907 doi:10.1103/PhysRevC.101.044907 [arXiv:1910.07678 [nucl-ex]].
67. Sahoo R., Association of Asia Pacic Physical Societies Bulletin 29(4), 16